Journal Pre-proof

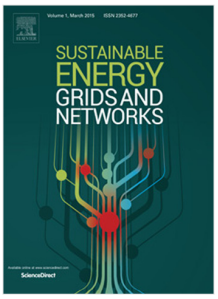

Distributionally robust decarbonizing scheduling considering data-driven ambiguity sets for multi-temporal multi-energy microgrid operation

Miaorui Ma, Chengwei Lou, Xiangmin Xu, Jin Yang,
Jake Cunningham, Lu Zhang

PII: S2352-4677(24)00052-3
DOI: https://doi.org/10.1016/j.segan.2024.101323
Reference: SEGAN 101323

To appear in: *Sustainable Energy, Grids and Networks*

Received date : 19 December 2023
Revised date : 18 January 2024
Accepted date : 12 February 2024

Please cite this article as: M. Ma, C. Lou, X. Xu et al., Distributionally robust decarbonizing scheduling considering data-driven ambiguity sets for multi-temporal multi-energy microgrid operation, *Sustainable Energy, Grids and Networks* (2024), doi: https://doi.org/10.1016/j.segan.2024.101323.

Revised manuscript (clean version) -PDF file for review

Graphical Abstract

Distributionally robust decarbonizing scheduling considering data-driven ambiguity sets for multi-temporal multi-energy microgrid operation

Miaorui Ma, Chengwei Lou, Xiangmin Xu, Jin Yang, Jake Cunningham, Lu Zhang

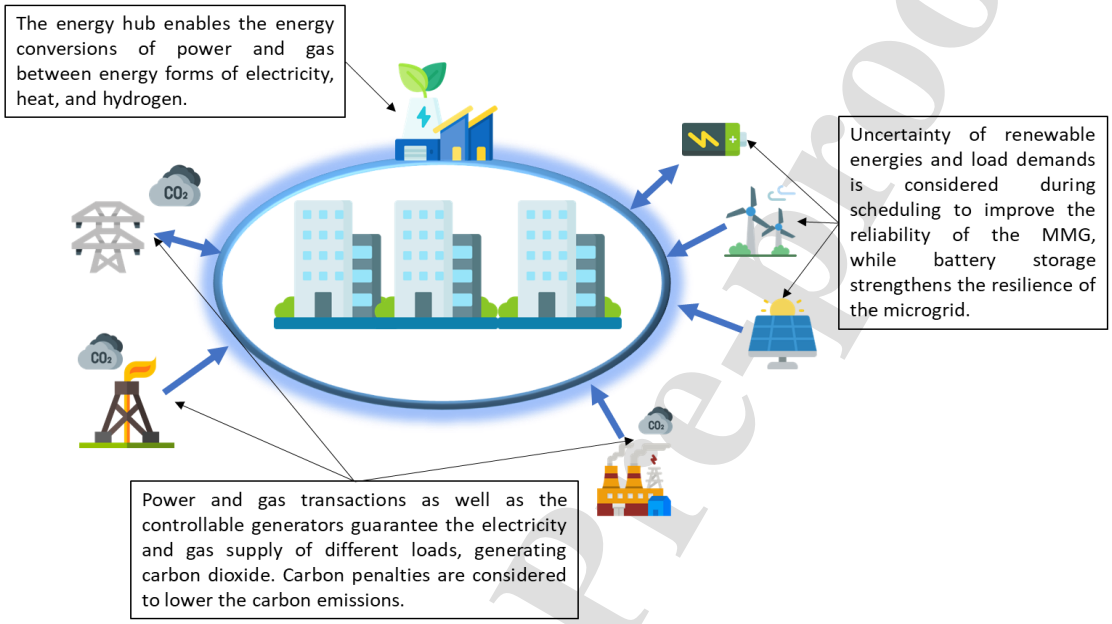

Distributionally robust decarbonizing scheduling considering data-driven ambiguity sets for multi-temporal multi-energy microgrid operation

Miaorui Ma[a], Chengwei Lou[a,b,*], Xiangmin Xu[a], Jin Yang[a], Jake Cunningham[a] and Lu Zhang[b]

[a]University of Glasgow, Glasgow, G12 8QQ, United Kingdom
[b]China Agricultural University, Beijing, China

ARTICLE INFO

Keywords:
Low-carbon technologies
Multi-energy microgrid
Multi-temporal
Data-driven
Distributionally robust optimization

ABSTRACT

As concerns about environmental sustainability continue to grow, the demand for effective low-carbon energy management becomes increasingly pressing. This study presents a novel framework for multi-temporal multi-energy microgrids (MMGs), integrating advanced low-carbon technologies to meet this imperative. The framework ensures flexible operations to navigate uncertainties stemming from renewable energy sources (RES) and fluctuating energy demand. Facilitating multi-energy transactions, encompassing gas and power exchanges in both markets, the model accommodates uncertainties from RES and demand fluctuations. Objectives include reducing carbon emissions and improving economic efficiency. To address uncertainties in the MMG system, a data-driven distributionally robust optimization (DRO) method is employed. Day-ahead scheduling utilizes a two-stage three-level approach, deploying the column-and-constraints generation (C&CG) algorithm, showcasing the efficiency of DRO in minimizing energy waste and carbon emissions while remaining cost-effective. Practicality is demonstrated through real-time intra-day scheduling using the model predictive control (MPC) algorithm, building upon hourly day-ahead results. The effectiveness of both strategies is evaluated using empirical data from an MMG based on the IEEE 33-bus test system. This cost-saving framework not only achieves a significant carbon reduction of 10.6 % but also provides reliable and adaptable solutions, effectively addressing real-world variations in renewable energy and mitigating potential risks.

1. Introduction

1.1. Background and Motivation

Mounting concerns about global warming have prompted efforts in the energy sectors to reduce carbon emissions, i.e. decarbonization [1]. In this context, renewable energy sources (RESs) and relevant technologies have prevailed, where wind and solar prove to be two viable alternatives for generating electricity with reduced carbon emissions [2]. Nevertheless, as the penetration of RES continues to rise, the accompanying uncertainties pose the risk of significant, unforeseen challenges in effective RES dispatching. At the same time, new ways to consume energy in heating (heat pumps) and transport (electric vehicles) introduce greater complexity. As a result, these uncertainties could create significant challenges in the management and operational aspects of energy systems, potentially putting the overall reliability of critical infrastructure (e.g. the power grid) at risk [3].

Multi-energy systems play an important role in decarbonization, whilst increasing energy conversion efficiency and system integration [4]. One representation of multi-energy systems is based on the energy hub (EH), where proficient and flexible advancement is fully exploited as a promising and strategically sound approach. An EH acts as a central hub for the smooth integration and efficient management of different energy demands, including electricity, heating/cooling, and transportation. Importantly, it can flexibly incorporate critical elements such as demand response, energy storage, and the seamless exploitation of various RESs. Such a holistic strategy not only ensures the effective management and control of multi-energy forms/resources but also lends itself to the development of a robust framework within the domain of sustainable energy systems [5].

Whilst capable of dealing with them, multi-energy systems encounter uncertainties associated with intermittent renewable resources, potentially impeding their ability to maintain steady operation. In existing research, robust optimization (RO) is widely used for optimizing under conditions of uncertainty, the main concept of which involves establishing a set of potential outcomes for uncertain parameters and subsequently optimizing based on the worst outcome within this set. However, the RO tends to be conservative as the uncertainty set includes worst-case scenarios [6]. Therefore, the development of an uncertainty optimization model and methodology becomes crucial in providing low-carbon multi-energy management solutions that account for uncertain renewable power generation and load conditions [7].

In response to these challenges, distributionally robust optimization (DRO) emerges as a promising approach. It combines the cost-effectiveness of stochastic optimization

*Corresponding author
m.ma.1@research.gla.ac.uk (M. Ma); chengwei.lou@cau.edu.cn; chengwei.lou@glasgow.ac.uk (.C. Lou); x.xu.1@research.gla.ac.uk (.X. Xu); jin.yang@glasgow.gla.ac.uk (.J. Yang); jake.cunningham@glasgow.gla.ac.uk (.J. Cunningham); zhanglu1@cau.edu.cn (.L. Zhang)
ORCID(s): 0009-0008-3753-0394 (M. Ma); 0000-0002-6224-0312 (.C. Lou); 0000-0002-3460-8212 (.X. Xu); 0000-0002-1026-8495 (.J. Yang)

Nomenclature

Acronyms

BS	Battery Storage
CG	Controllable Generator
CHP	Combined Heat and Power
EH	Energy Hub
ET	Energy Turbine
GT	Gas Turbine
P2G	Power to Gas
PV	Photovoltaic
TF	Transformer
WT	Wind Turbine

Parameters

η_{ET}	ET energy conversion coefficient
η_{GT}	GT energy conversion coefficient
η_{P2G}	P2G energy conversion coefficient
η_{TF}	TF energy conversion coefficient
$\eta_{B,\mathrm{dis}}$,$\eta_{B,\mathrm{ch}}$	Battery storage discharging and charging efficiency coefficient
η_{ce}	Power conversion coefficient of CHP
η_{ch}	Heat conversion coefficient of CHP
$\lambda_{\mathrm{BS},t}^{intra}$	Cost coefficient for the difference of day-ahead and intra-day cost of battery storage
$\lambda_{\mathrm{CO2},t}^{G}$	Cost factor for carbon emission generated by gas purchase
$\lambda_{\mathrm{CO2},t}^{P}$	Cost factor for carbon emission generated by power purchase and CG generation
$\lambda_{G,t}$	Gas price
$\lambda_{M,t}$	Power transaction price
$\lambda_{M,t}^{intra}$	Cost coefficient for the difference of day-ahead and intra-day cost of power transaction
A,B	The operation cost factor of the CG and the energy hub
C_{ud}	Start-stop cost of CG
$c_{w,t}^{WTP}$, $c_{p,t}^{PVP}$	Penalty cost factor for wind and solar curtailment
$E_B^{SOC,\max}$,$E_B^{SOC,\min}$	The upper limit and lower limit of the energy that the energy storage facility can store at time t
$G_{\mathrm{CHP}}^{\max}$, $G_{\mathrm{CHP}}^{\min}$	The maximum and minimum output of CHP
$G_{\mathrm{GT}}^{\max}$, $G_{\mathrm{GT}}^{\min}$	The maximum and minimum output of GT
K_{BS}	The charging and discharging cost factor of battery storage
$N_{B,\mathrm{BS}}^{lim}$	The maximum charge and discharge state transition times of energy storage
$P_{\mathrm{CG}}^{\max}$, $P_{\mathrm{CG}}^{\min}$	Maximum and minimum active power of CG
$P_{\mathrm{EH},t}$	Power output of the energy hub
$P_{\mathrm{ET}}^{\max}$, $P_{\mathrm{ET}}^{\min}$	The maximum and minimum output of ET
$P_{\mathrm{P2G}}^{\max}$, $P_{\mathrm{P2G}}^{\min}$	The maximum and minimum output of P2G
$P_{\mathrm{SUB}}^{\max}$, $G_g^{\max}$	The maximum limit of power and gas transaction
$P_{\mathrm{TF}}^{\max}$, $P_{\mathrm{TF}}^{\min}$	The maximum and minimum output of TF
$P_{B,\mathrm{BS}}^{\max,\mathrm{ch}}$,$P_{B,\mathrm{BS}}^{\min,\mathrm{ch}}$	Upper and lower limits of charging power
$P_{B,\mathrm{BS}}^{\max,\mathrm{dis}}$,$P_{B,\mathrm{BS}}^{\min,\mathrm{dis}}$	Upper and lower limits of discharging power
R^{up}, R^{down}	Upper and lower bounds on ramping rate
$\mathrm{S}_{G,t}$	Start-stop cost factor

Sets

B_e^{BS}	Set of battery storage system
U_w, U_p	The uncertainty set of wind and solar energy

Variables

$\Delta E_{M,t}, \Delta E_{\mathrm{BS},t}$	The difference of day-ahead and intra-day power transaction and battery storage at time t
$C_{\mathrm{BS},t}, C_{\mathrm{BS},t}^{intra}$	Day-ahead and intra-day cost of battery storage systems
$C_{\mathrm{CG},t}, C_{\mathrm{CG},t}^{intra}$	Day-ahead and intra-day cost of CG operation
$C_{\mathrm{CO2},t}, C_{\mathrm{CO2},t}^{intra}$	Day-ahead and intra-day carbon cost
$C_{\mathrm{EH},t}, C_{\mathrm{EH},t}^{intra}$	Day-ahead and intra-day operation cost of energy hub
$C_{\mathrm{PV},t}, C_{\mathrm{PV},t}^{intra}$	Day-ahead and intra-day cost of solar curtailment
$C_{\mathrm{WT},t}, C_{\mathrm{PV},t}$	The cost of wind and solar curtailment at time t
$C_{\mathrm{WT},t}, C_{\mathrm{WT},t}^{intra}$	Day-ahead and intra-day cost of wind curtailment
$C_{G,t}, C_{G,t}^{intra}$	Day-ahead and intra-day cost of gas purchase
$C_{M,t}, C_{M,t}^{intra}$	Day-ahead and intra-day cost of power transaction
$E_{\mathrm{BS},t}^{intra}$, $E_{\mathrm{BS},t}^{ahead}$	The intra-day and day-ahead battery storage energy at time t
$E_{B,t}^{SOC}$	The energy stored in the energy storage device connected to node B at time t
$E_{M,t}^{intra}$, $E_{M,t}^{ahead}$	The intra-day and day-ahead power transaction at time t
$G_{\mathrm{CHP},t}, G_{\mathrm{CHP},t-1}$	The output of CHP at time t and t-1
$G_{\mathrm{GT},t}, G_{\mathrm{GT},t-1}$	The output of GT at time t and t-1
$G_{buy,t}$	Gas Purchase
P, P_{cp}, P_{cg}	Real-time power price, carbon penalty price of power and gas
$P_{\mathrm{CG},t}, P_{\mathrm{CG},t-1}$	Active power output of controllable generators at time t and t-1
$P_{\mathrm{CG},t}^{intra}$	Intra-day CG generation
$P_{\mathrm{ET},t}, P_{\mathrm{ET},t-1}$	The output of ET at time t and t-1
$P_{\mathrm{P2G},t}, P_{\mathrm{P2G},t-1}$	The output of P2G at time t and t-1
$P_{\mathrm{PV},t}^{*}, P_{\mathrm{PV},t}$	The predicted and real output power of solar power at time t
$P_{\mathrm{SUB},t}$	Transmission power between the maingrid and the MMG
$P_{\mathrm{SUB},t}^{buy}$, $P_{\mathrm{SUB},t}^{sell}$	Purchase and sale of electricity between microgrid and distribution network
$P_{\mathrm{TF},t}, P_{\mathrm{TF},t-1}$	The output of TF at time t and t-1
$P_{\mathrm{WT},t}^{*}, P_{\mathrm{WT},t}$	The predicted and real output power of wind power at time t
$P_{B,t}^{\mathrm{sum,dis}}$,$P_{B,t}^{\mathrm{sum,ch}}$	The discharging and charging power of the battery
$u_{\mathrm{SUB},t}$	The status of power transaction from microgrid to distribution network in grid-connected operation mode
$u_{B,t}^{\mathrm{dis}}$,$u_{B,t}^{\mathrm{ch}}$	Charging and discharging status of energy storage
$u_{G,t}, u_{G,t-1}$	Start-stop status of CG at time t and t-1
$v_{M,t}$	Operation mode of micro-grid, island mode or grid-connected mode

(SO) and the conservativeness of RO, which seeks to strike a balance between minimizing energy costs and ensuring system resilience [8]. To address the multi-energy system scheduling challenges, this paper presents a novel framework based on multi-energy microgrid (MMG). Within this framework, a day-ahead dispatch model employing the DRO method is formulated, which is subsequently applied to the MMG system, with dual consideration for the essential objectives of decarbonizing and cost-efficiency. To increase the practical significance of the proposed methodology, the intra-day scheduling following the day-ahead scheduling outcomes is implemented.

1.2. Literature Review

At the microgrid level, the majority of existing research primarily concentrates on the functionality of individual energy microgrids [9], [10], [11], without discussing the incorporation of multiple energy sources. To increase the system operating efficiency and dispatch flexibility, [12] proposes a comprehensive system-wide optimal coordinated dispatch method for the MMG in both grid-connected and islanding modes. The objectives are to optimize the net operational cost of the microgrid in both modes while adhering to the system's operational constraints. In [13], a general modeling approach for the steady-state energy balance equation of multi-energy systems is presented. This approach includes the incorporation of energy converters, energy storage, and renewable energy devices. [14] constructs a multi-scenario operation optimization model for a park integrated energy system based on multi-energy demand response (DR), of which the energy utilization efficiency and net system profit show improvements of 2.30% and 2,652.775$ respectively, compared to the conventional scenario. A multi-period dispatch model using improved particle swarm optimization (IPSO) is proposed in [15], which takes into account the potential profit from energy storage systems, the results of which demonstrate that the dispatch strategy successfully lowers the overall operational costs and provides improved scheduling of distributed generation units in grid-connected MMGs.

To consider environmental factors, the objective of [16] is to investigate the environmental economic dispatch for large-scale integrated energy systems (IESs), specifically in the integrated regional energy systems with coal, gas, combined heat and power (CHP), and RES systems, taking into account the influence of air pollutant control technologies and DR programs on the system. [17] proposes a low-carbon operation method for microgrids with the consideration of carbon emission quota trading. [18] presents an optimized energy management strategy to minimize an MMG network's operational expenses. The strategy takes into account operational constraints and carbon emissions in the decision-making process. Additionally, [19] proposes a framework aimed at assisting aggregators in the real-time provision of network-secure and multi-energy services. This framework takes into account the integration of green hydrogen and measures for carbon reduction.

In the above-mentioned literature [12] to [19], the multi-energy coordination is based on the deterministic day-ahead operation. However, they neglect uncertainties related to RES outputs, power loads, and transaction prices, which limits practicality for real-world applications. Guan et al. [20] put forward an alternate method to tackle these uncertainties. The SO techniques are used to minimize the power and natural gas expenses at the building level while considering the uncertain outputs of RES and power loads. This methodology takes into account the uncertainties, rendering it more feasible for real-world implementations. Experimental outcomes demonstrate substantial cost reductions attained in energy expenses by employing integrated scheduling and control of diverse building energy supply sources. [21] utilizes the Latin Hypercube Sampling method to manage uncertainties in energy carriers including power, heat, and hydrogen. The study introduces a decentralized bi-level SO method using the progressive hedging algorithm for multi-agent systems in MMGs, aiming to enhance network flexibility and improve the system's overall performance. A temporally-coordinated optimal operation method for microgrids is solved by mixed integer linear programming (MILP) and a multi-stage stochastic operation method is proposed to handle the uncertainties [22]. Similarly, MILP is also applied in [23] to solve the optimal scheduling problem for microgrids. A hybrid robust/stochastic framework is also proposed to address high-level uncertainty. Column-and-constraint generation (C&CG) algorithm is applied in [24] to solve a DRO model considering the uncertainties of renewable energy sources.

From the perspective of low-carbon performance in power systems with uncertainties considered, authors in [25] propose a dynamic economic dispatch model with the assistance of the particle swarm optimization (PSO) algorithm to solve the power dispatching problem with a dual consideration of wind power uncertainty and carbon emission rights in a low-carbon setting. [26] focuses on the integrated energy system and develops a day-ahead low-carbon two-stage dispatch model applied to a regionally integrated energy system. Different from those at the microgrid level, this research considers purchasing electricity from the main grid and does not involve bi-directional transactions. This research also quantifies the impacts of wind/PV penetration, carbon price, and scenario numbers.

1.3. Research Gap

Despite the extensive research in microgrid scheduling and management, there is a noticeable research gap concerning the development of comprehensive strategies for low-carbon MMGs. Existing approaches lack in accurately emulating the operations of real power distribution systems and responding promptly to dynamic changes in energy supply and demand, limiting their practicality. Additionally, the uncertainty associated with renewable energies poses a significant challenge to achieving robust carbon reduction goals, requiring precise control at shorter intervals for

Table 1
Comparison among different research work on the management strategies of the MMG.

References	Energy Carriers				RES		Uncertainty Modelling	Algorithm	Timescale	Carbon Trade
	Power	Gas	Heat	Hydro	PV	WT				
[12]								MILP	hourly	
[13]								MINLP	hourly	
[14]								MILP	hourly	
[15]								IPSO	hourly	
[16]								MILP	hourly	
[17]								MILP	hourly	
[18]								MILP and MIQP	hourly	
[19]								MPC	hourly & 20s	
[20]							Stochastic	MILP	hourly	
[21]							Latin Hypercube Sampling	Bi-Level Stochastic	hourly	
[22]							Stochastic	MILP	hourly & 5-min	
[23]							Hybrid Robust/Stochastic	MILP	hourly	
[24]							Data-Driven Set Based RO	C&CG	hourly	
[25]							Random Sampling	PSO	hourly	
Proposed Model							Data-Driven Set Based RO	C&CG and MPC	hourly & 15-min	

seamless integration. The optimization problem for multi-temporal scheduling in low-carbon MMG, considering uncertainties in renewable energies, is insufficiently explored.

Closing this gap is pivotal for the development of robust and decarbonizing scheduling strategies for MMGs, and this study aims to contribute by addressing this research limitation. To effectively tackle this research gap, it is imperative to advance energy management strategies and technologies. These advancements should possess the capability to seamlessly integrate and harness the full potential of renewable resources, ensuring both system reliability and environmental sustainability. Hence, there exists a critical need to formulate an advanced and efficient framework for a comprehensive low-carbon scheduling approach with multi-temporal resolution. This framework will play a pivotal role in optimizing MMG operations and aligning economic efficiency with environmental objectives in the context of the microgrid.

In Table 1, we present a thorough comparison of different reported pieces of research work on the management strategies of microgrids, from the aspects of 1) allowed forms of energy carriers, 2) considered types of RES, 3) uncertainty modeling, 4) timescales, 5) enabled carbon trading, and 6) solving algorithms. It can be found that so far there is little literature published to fully consider key factors such as 1)-5).

1.4. Contributions of This Paper

Therefore, in this paper, we propose a new decarbonizing data-driven robust optimal scheduling framework for an MMG that consists of wind turbines (WT), photovoltaic (PV) cells, controllable generators (CG), battery storage systems, and energy hubs. The objective is to minimize the daily total cost over a 24-hour horizon, which includes power and gas transactions, CG operational costs, battery storage charging and discharging costs, and carbon costs. As shown in Table 1, it is so far the most comprehensive work that allows all key factors to be fully considered, in particular the integrated energy forms with uncertainties, highlighting carbon reduction requirements.

In this framework, we employ a two-step approach as shown in Fig. 1. First, the day-ahead scheduling is formulated into a DRO problem and solved by C&CG. It plans hourly for energy dispatch considering uncertainties from the probability distribution generated from clustered data of renewable energies and load demand. Subsequently, in the intra-day scheduling phase, adjustments are made to align with the day-ahead scheduling decisions every 15 minutes solved by model predictive control (MPC), aiming to minimize discrepancies and reduce scheduling losses. This approach develops an innovative framework integrating advanced algorithms for multi-temporal, multi-energy microgrid scheduling, with a specific focus on uncertainty modeling and decarbonizing operations. This involves clustering a significant amount of historical data and conducting a detailed analysis of dispatch results across different time scales, which distinguishes our work as a practical and decarbonizing optimal scheduling for MMGs. The specific contributions of this paper are summarized as follows:

1.**A fully considered MMG with operational uncertainty**: To enhance the cost-effectiveness of grid dispatch operations and minimize energy waste, our paper focuses on a novel approach that rigorously addresses uncertainties inherent in both day-ahead and real-time grid dynamics. Specifically, our model incorporates factors such as RES outputs and load fluctuations and aligns the MMG more closely with complex real-world scenarios, which not only contributes to a more reliable MMG but also significantly improves its practical applicability.

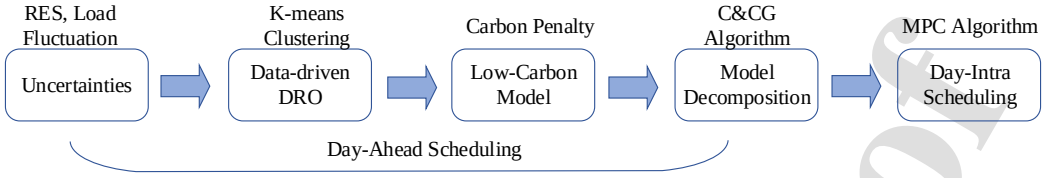

Figure 1: Framework of the 2-Step Approach and Research Methodology.

2. **A carbon penalty (CP), in consideration of the above uncertainty**: Based on considering the uncertainties of the MMG, we introduce the concept of CP. CP is calculated based on carbon factors associated with different energy sources and is optimized as part of the objective function. Additionally, we analyze the carbon emissions and costs under different carbon prices to achieve an optimal solution for reducing total costs and carbon emissions.

3. **A proposed multi-temporal method with adapted algorithms**: To implement the model put forth in this article, the advanced and efficient DRO method is employed. Additionally, the C&CG algorithm is leveraged to derive the optimal solution for hourly day-ahead power grid dispatching. In a bid to validate its real-time applicability, the intra-day dispatch results in 15-minute intervals are calculated through the utilization of the MPC algorithm, achieving optimal intra-day scheduling.

The remainder of this paper is organized as follows. Section 2 presents the formulation models of components of the MMG system. Section 3 illustrates the DRO mathematical model of the MMG day-ahead scheduling problem with the uncertainty set. Section 4 introduces the 2-step scheduling including the C&CG algorithm for day-ahead scheduling and the MPC algorithm for intra-day scheduling. The results of numerical calculations are presented in Section 5, while Section 6 concludes this paper.

2. Model Formulation

2.1. Configuration of the MMG

As a microgrid with multi-energy capabilities, the system represented in Fig. 2 should be able to self-sustain in islanding mode or draw electricity from the main grid. The heart of this system lies in its energy hubs (EH), which contain dual energy forms of electricity and gas. The electricity network caters to hydrogen, electric-heating, and electrical loads while the gas network attends to the hydrogen and gas-heating requirements. Hydrogen loads can be included through a power-to-gas (P2G) process. Heat loads, on the other hand, are fulfilled by an energy turbine (ET), CHP systems, and a gas turbine (GT). Electrical loads are satisfied through a controllable/dispatchable generator (CG), transactions with the main grid, battery storage (BS), and RES systems. The system's carbon footprint stems principally from three sources: the primary grid, gas network, and CGs.

2.2. Component Modeling

As this study focuses on the operation of the multi-energy microgrid, the corresponding cost functions and constraints that each component needs to satisfy during the operation of the microgrid will be introduced and modeled separately in this section.

(1) Battery Storage

i. Cost Function

The average charging and discharging cost of battery storage is:

$$C_{\mathrm{BS,t}} = \sum_{B \in B_e^{\mathrm{BS}}} \{ K_{\mathrm{BS}} \left[\frac{1}{\eta_{B,\mathrm{dis}}} P_{B,t}^{\mathrm{sum,dis}} + \eta_{B,\mathrm{ch}} P_{B,t}^{\mathrm{sum,ch}} \right] \} \Delta t \quad (1)$$

where Δt is the scheduling step.

ii. Constraints

The charging and discharging power of energy storage need to satisfy the maximum and minimum limit constraints:

$$u_{B,t}^{\mathrm{ch}} P_{B,\mathrm{BS}}^{\mathrm{min,ch}} \le P_{B,t}^{\mathrm{sum,ch}} \le u_{B,t}^{\mathrm{ch}} P_{B,\mathrm{BS}}^{\mathrm{max,ch}} \quad (2)$$

$$u_{B,t}^{\mathrm{dis}} P_{B,\mathrm{BS}}^{\mathrm{min,dis}} \le P_{B,t}^{\mathrm{sum,dis}} \le u_{B,t}^{\mathrm{dis}} P_{B,\mathrm{BS}}^{\mathrm{max,dis}} \quad (3)$$

Logically, energy storage can only work in one of the states of charging or discharging. Therefore, the binary variables indicating the status of charging $u_{B,t}^{\mathrm{ch}}$ and discharging $u_{B,t}^{\mathrm{dis}}$ cannot both be 1 at the same time:

$$u_{B,t}^{\mathrm{ch}} + u_{B,t}^{\mathrm{dis}} \le 1 \quad (4)$$

The number of transitions between charge and discharge states should be less than the maximum transition numbers.

$$\sum_{t} \left| u_{B,t}^{\mathrm{dis}} - u_{B,t-1}^{\mathrm{dis}} \right| \le N_{B,\mathrm{BS}}^{lim} \quad (5)$$

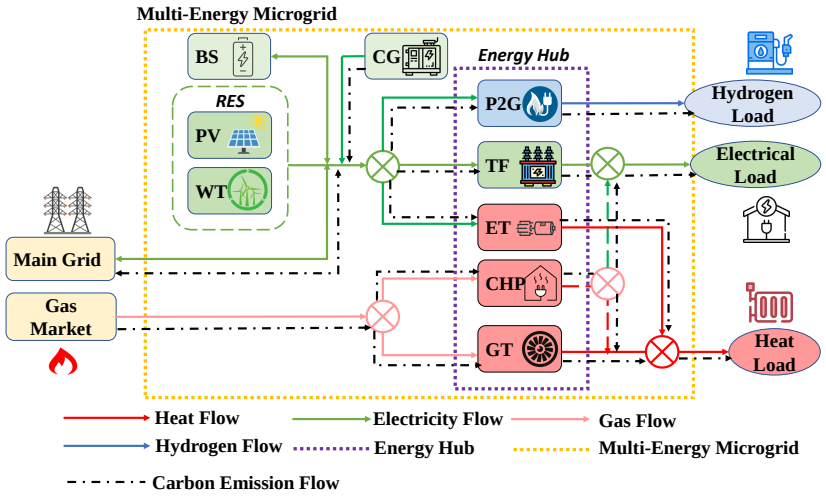

Figure 2: A Representative MMG Configuration.

The State-of-Charge (SOC) of battery storage at time t can be represented as below:

$$E_{B,t}^{SOC} = E_{B,t-1}^{SOC} - \frac{1}{\eta_{B,\text{dis}}} P_{B,t}^{\text{sum,dis}} \Delta t + \eta_{B,\text{ch}} P_{B,t}^{\text{sum,ch}} \Delta t \quad (6)$$

$$E_{B}^{SOC,\min} \le E_{B,t}^{SOC} \le E_{B}^{SOC,\max}, \forall t \in T \quad (7)$$

(2) Controllable Generation

i. Cost Function

The start-up and shut-down cost of CG can be written as:

$$C_{ud} = [\max\{0, u_{G,t} - u_{G,t-1}\} S_{G,t}] \Delta t \quad (8)$$

The operation cost of a controllable generator is:

$$C_{\text{CG},t} = A P_{\text{CG},t} \Delta t \quad (9)$$

where A is the price of CG operation, £/kWh.

ii. Constraints

The maximum and minimum output of controllable generators can be restricted as:

$$u_{G,t} P_{\text{CG}}^{\min} \le P_{\text{CG},t} \le u_{G,t} P_{\text{CG}}^{\max} \quad (10)$$

Additionally, the controllable generators should meet the ramping constraints:

$$P_{\text{CG},t} - P_{\text{CG},t-1} \le R^{up} \Delta t \quad (11)$$

$$P_{\text{CG},t-1} - P_{\text{CG},t} \le R^{down} \Delta t \quad (12)$$

(3) Mutual Transactions

i. Cost Function

Power transaction cost between the micro-grid and distribution grid can be described as:

$$P_{\text{SUB},t} = P_{\text{SUB},t}^{buy} - P_{\text{SUB},t}^{sell} \quad (13)$$

$$C_{M,t} = [\lambda_{M,t} P_{\text{SUB},t}] \Delta t \quad (14)$$

where $\lambda_{M,t}$ is the time-varying price of power transaction, £/kWh.

And the gas purchase can be expressed as:

$$C_{G,t} = [\lambda_{G,t} Q_{buy,t}] \Delta t \quad (15)$$

where $\lambda_{G,t}$ is the time-varying price of gas purchase, £/kWh.

ii. Constraints

The maximum purchase and selling of electricity at time t should also be restrained:

$$0 \le P_{\text{SUB},t}^{buy} \le \upsilon_{M,t} u_{\text{SUB},t} P_{\text{SUB}}^{\max} \quad (16)$$

$$0 \le P_{\text{SUB},t}^{sell} \le \upsilon_{M,t} [1 - u_{\text{SUB},t}] P_{\text{SUB}}^{\max} \quad (17)$$

The maximum purchase and selling of gas at time t should be restricted in (18):

$$0 \le G_{g,t}^{buy} \le G_{g}^{\max} \quad (18)$$

(4) Renewable Energy Generation

i. Cost Function

Wind and solar energy curtailment penalties at time t can be expressed as:

$$C_{\text{WT},t} = \sum_{w \in U_w} \{c_{w,t}^{WTP} [P_{\text{WT},t}^{*} - P_{\text{WT},t}]\} \Delta t \quad (19)$$

$$C_{\mathrm{PV},t} = \sum_{p\in U_p} \{c_{p,t}^{PVP}[P_{\mathrm{PV},t}^{*} - P_{\mathrm{PV},t}]\}\Delta \mathrm{t} \tag{20}$$

(5) Energy Hub

i. Cost Function

Assuming the EH is an integrated system, the start-stop cost is constant and included in $S_{G,t}$. The operation cost of EH can be expressed as a linear function:

$$C_{\mathrm{EH},t} = BP_{\mathrm{EH},t}\Delta \mathrm{t} \tag{21}$$

where B is the operational cost factor of EH equipment.

ii. Constraints

The maximum and minimum limits of EH facilities, which include CHP, GT, P2G, TF, and ET are defined by equation (22) to (26):

$$G_{\mathrm{CHP}}^{\min} \le G_{\mathrm{CHP},t} \le G_{\mathrm{CHP}}^{\max} \tag{22}$$
$$G_{\mathrm{GT}}^{\min} \le G_{\mathrm{GT},t} \le G_{\mathrm{GT}}^{\max} \tag{23}$$
$$P_{\mathrm{P2G}}^{\min} \le P_{\mathrm{P2G},t} \le P_{\mathrm{P2G}}^{\max} \tag{24}$$
$$P_{\mathrm{TF}}^{\min} \le P_{\mathrm{TF},t} \le P_{\mathrm{TF}}^{\max} \tag{25}$$
$$P_{\mathrm{ET}}^{\min} \le P_{\mathrm{ET},t} \le P_{\mathrm{ET}}^{\max} \tag{26}$$

The corresponding ramping constraints of these facilities are also defined by equation (27) to (36):

$$G_{\mathrm{CHP},t} - G_{\mathrm{CHP},t-1} \le R^{up}\Delta \mathrm{t} \tag{27}$$
$$G_{\mathrm{GT},t} - G_{\mathrm{GT},t-1} \le R^{up}\Delta \mathrm{t} \tag{28}$$
$$P_{\mathrm{P2G},t} - P_{\mathrm{P2G},t-1} \le R^{up}\Delta \mathrm{t} \tag{29}$$
$$P_{\mathrm{TF},t} - P_{\mathrm{TF},t-1} \le R^{up}\Delta \mathrm{t} \tag{30}$$
$$P_{\mathrm{ET},t} - P_{\mathrm{ET},t-1} \le R^{up}\Delta \mathrm{t} \tag{31}$$
$$G_{\mathrm{CHP},t-1} - G_{\mathrm{CHP},t} \le R^{down}\Delta \mathrm{t} \tag{32}$$
$$G_{\mathrm{GT},t-1} - G_{\mathrm{GT},t} \le R^{down}\Delta \mathrm{t} \tag{33}$$
$$P_{\mathrm{P2G},t-1} - P_{\mathrm{P2G},t} \le R^{down}\Delta \mathrm{t} \tag{34}$$
$$P_{\mathrm{TF},t-1} - P_{\mathrm{TF},t} \le R^{down}\Delta \mathrm{t} \tag{35}$$
$$P_{\mathrm{ET},t-1} - P_{\mathrm{ET},t} \le R^{down}\Delta \mathrm{t} \tag{36}$$

(6) Carbon Penalty

i. Cost Function

The carbon emission is mainly embedded in three parts: the power purchase, the gas purchase, and the CG output. The carbon emissions of EH are encompassed in the gas transactions. Therefore, the CP cost can be expressed as:

$$C_{\mathrm{CO2},t} = [\lambda_{\mathrm{CO2},t}^{P}(P_{\mathrm{SUB},t}^{buy} + P_{\mathrm{CG},t}) + \lambda_{\mathrm{CO2},t}^{G}G_{g,t}^{buy}]\Delta \mathrm{t} \tag{37}$$

(7) Power Balance

From Figure 2, the power balance can be expressed in general as below:

$$P_{\mathrm{CG},t} + P_{\mathrm{PV},t} + P_{\mathrm{WT},t} + P_{B,t}^{\mathrm{dis,sum}} + P_{\mathrm{SUB},t} = P_{\mathrm{P2G},t} + P_{\mathrm{TF},t} + P_{\mathrm{ET},t} + P_{B,t}^{\mathrm{ch,sum}} \tag{38}$$
$$G_{buy,t} = G_{\mathrm{CHP},t} + G_{\mathrm{GT},t} \tag{39}$$
$$P_{\mathrm{LG},t} = \eta_{\mathrm{P2G}}P_{\mathrm{P2G},t} \tag{40}$$
$$P_{\mathrm{LE},t} = \eta_{\mathrm{TF}}P_{\mathrm{TF},t} + \eta_{ce}G_{\mathrm{CHP},t} \tag{41}$$
$$P_{\mathrm{LH},t} = \eta_{\mathrm{ET}}P_{\mathrm{ET},t} + \eta_{\mathrm{ch}}G_{\mathrm{CHP},t} + \eta_{\mathrm{GT}}G_{\mathrm{GT},t} \tag{42}$$

3. Proposed Framework of Decarbonizing Data-driven DRO Mathematical Model

3.1. Mathematical Model of Day-Ahead Scheduling Problem

In this study, we employ a data-driven DRO approach for day-ahead scheduling to characterize the uncertainty associated with load demand and the RES system, specifically accounting for wind and solar power uncertainties. Utilizing empirical data, the K-means clustering algorithm is leveraged to generate K scenarios with initial probabilities.

Given that the actual distribution often deviates from the aforementioned distribution, a nuanced approach is adopted. Instead of solely relying on either the norm-1 or norm-inf separately to constrain the probability distribution, we simultaneously consider both norms. This approach culminates in the formation of an uncertain probability confidence set, guided by the constraints imposed by the comprehensive norm [27].

The overall structure of the data-driven distributionally robust day-ahead optimal scheduling model can be succinctly formulated in a two-stage matrix representation, as articulated in [28]. This study takes the start-stop status as the first-stage decision variable to instruct the dispatch scheduling, which cannot be adjusted after the uncertainties are revealed [27]. The second-stage variables stand for the operation decisions. The primary objective, as represented by the equation below, entails the minimization of start-up and shut-down costs, operational expenditures, and capacity payment costs, while simultaneously ensuring adherence to all equality and inequality constraints, where $a^T x$ is the start-up and shunt-down cost, and $b^T y_k$ represents the operational cost and CP.

$$\min_{x\in X}[a_T x + \max_{p_k\in\Omega}\sum_{k=1}^{K} p_k \min_{y_{k\in Y(x,\xi_k)}} b^T y_k] \tag{43}$$
$$s.t.\ Ax \le d \tag{44}$$
$$Bx = e \tag{45}$$
$$Cy_k \le D\xi_k, \forall\ k = 0,\ \ldots, K \tag{46}$$
$$Gx + Hy_k \le g, \forall\ k = 0,\ \ldots, K \tag{47}$$

$$Jx + Ky_k = h,\ \forall\ k = 0,\ \ldots, K \tag{48}$$

3.2. Confidence Set of Day-Ahead Scheduling Model

In the DRO day-ahead scheduling model, there is uncertainty in the probabilities of various discrete scenarios. To ensure that the probability distribution of scenarios fluctuates within a reasonable range, the probability distributions of forecast errors in the output of renewable energy sources and load demand, are defined as sets of uncertainties. The confidence set is constructed as follows [27]:

$$\Omega = \left\{ \{p_k\} \left| \begin{array}{c} p_k \geq 0,\ k = 1, \ldots, K \\ \sum_{k=1}^{K} p_k = 1 \\ \sum_{k=1}^{K} \left| p_k - p_k^0 \right| \leq \theta_1 \\ \max_{1\leq k\leq K} \left| p_k - p_k^0 \right| \leq \theta_\infty \end{array} \right. \right\} \tag{49}$$

where p_k^0 stands for the initial probability of the scenario k. The norm-1 and norm-inf are used to constrain the confidence set of probability distributions.

Taking both types of norm constraints into account avoids extreme situations. Norm-1 limits the upper bound of the sum of the allowable deviations of all scenario probability distributions, while the norm-inf limits each scenario probability distribution. Assuming there are K scenarios from M historical samples, to construct confidence constraints under different values θ according to the historical data and confidence level [28]:

$$Pr\left\{ \sum_{k=1}^{K} \left| p_k - p_k^0 \right| \leq \theta_1 \right\} \geq 1 - 2Ke^{-2M\theta_1/K} \tag{50}$$

$$Pr\left\{ \max_{1\leq k\leq K} \left| p_k - p_k^0 \right| \leq \theta_\infty \right\} \geq 1 - 2Ke^{-2M\theta_\infty} \tag{51}$$

Let the right-hand side of the above formula be the confidence degree of uncertainty probability α_1 and α_∞ respectively, the tolerance values of norm-1 and norm-inf for the DRO model can be obtained as:

$$\theta_1 = \frac{K}{2M} \ln \frac{2K}{1-\alpha_1} \tag{52}$$

$$\theta_\infty = \frac{1}{2M} \ln \frac{2K}{1-\alpha_\infty} \tag{53}$$

To linearize the absolute value constraint, a binary auxiliary variable z_s^+,z_s^- is introduced in the norm-1 constraints [28]:

$$\begin{cases} \sum_{k=1}^{K} (p_k^+ - p_k^-) \leq \theta_1 \\ p_k = p_k^0 + p_k^+ - p_k^- \\ z_k^+ + z_k^- \leq 1 \\ 0 \leq p_k^+ \leq z_k^+ \theta_1 \\ 0 \leq p_k^- \leq z_k^- \theta_1 \end{cases} \tag{54}$$

Also, introducing y_s^+,y_s^- in the norm-inf constraints:

$$\begin{cases} p_k^+ - p_k^- \leq \infty \\ p_k = p_k^0 + p_k^+ - p_k^- \\ y_k^+ + y_k^- \leq 1 \\ 0 \leq p_k^+ \leq y_k^+ \theta_\infty \\ 0 \leq p_k^- \leq y_k^- \theta_\infty \end{cases} \tag{55}$$

4. Mathematical Model of 2-Step Scheduling

4.1. First Step: C&CG Method for Day-Ahead Scheduling

The C&CG method is a relatively efficient algorithm [29]. The C&CG algorithm is applied to decompose the original problem into the main problem (MP) and sub-problem (SP). Iterative calculations are performed until the difference in the optimization results between MP and SP meets the set tolerance to solve the two-stage DRO problem.

(1) Master Problem

The MP is to minimize the optimal scheduling and CP cost under the condition that the worst-case scenario is known. It is a two-stage three-level optimization problem, solved by the C&CG algorithm in this study. The results of the MP provide the lower bound (LB) to the C&CG algorithm [29]. Then the first-stage decision variables can be passed to the SP for iteration calculations.

$$\min_{x\in X, y_k^m \in Y(x,\xi_k), L} a^T x + L \tag{56}$$

$$L \geq \sum_{k=1}^{K} p_k^m b^T y_k^m, \forall m = 1, 2, \ldots, n \tag{57}$$

where n is the iteration number.

(2) Sub-Problem

Under the condition that the first-stage decision variables are known, SP results provide the upper bound (UB) for the C&CG algorithm.

$$L(x^*) = \max_{p_k\in\Omega} p_k^m \min_{y_k^m \in Y(x^*,\xi_k)} b^T y_k^m, \forall m = 1, 2, \ldots, n \tag{58}$$

The inner level can be reformulated into:

$$L(x^*) = \max_{p_k\in\Omega} \sum_{k=1}^{K} p_k^m \eta_k \tag{59}$$

$$s.t.\ \eta_k = argmin(b^T y_k^m) \tag{60}$$

The inner level represents the optimal scheduling result under scenario k, while the outer level represents the worst expectation of each scenario. The inner model should be solved first, and the outer model is subsequently handled [29]. Meanwhile, the probability of each scenario under the worst expectation can be obtained after clustering.

4.2. Second Step: MPC Method for Intra-Day Scheduling

Based on the results of optimal 24-hour day-ahead scheduling, the MPC is applied to obtain intra-day scheduling. MPC includes model prediction, rolling optimization, and feedback correction, which has excellent tracking performance and anti-interference ability [30]. The scheduling step time interval for predicting the operation decision variables should be done in a 15-minute interval in the 2-hour ahead rolling horizon [31]. Only the first 15-minute decisions are adopted.

The start-up and shut-down status of CG should follow the day-ahead scheduling results. Therefore, the cost of CG start-stop should stay the same with the day-ahead scheduling results. The operational cost is:

$$C_{\mathrm{CG},t}^{intra} = A P_{\mathrm{CG},t}^{intra} \Delta t \tag{61}$$

Additionally, the charging and discharging power of battery storage during intra-day scheduling should try to follow day-ahead scheduling as well. The intra-day cost of the battery storage system is:

$$C_{\mathrm{BS},t}^{intra} = \sum_{B \in B_e^{\mathrm{BS}}} \{ K_{\mathrm{BS},i} \left[\frac{1}{\eta_{B,\mathrm{dis}}} P_{B,t}^{\mathrm{sum,dis}} + \eta_{B,\mathrm{ch}} P_{B,t}^{\mathrm{sum,ch}} \right] + \lambda_{\mathrm{BS}}^{intra} \Delta E_{\mathrm{BS},t} \} \Delta t \tag{62}$$

$$s.t. \Delta E_{\mathrm{BS},t} \geq E_{\mathrm{BS},t}^{intra} - E_{\mathrm{BS},t}^{ahead} \tag{63}$$

$$\Delta E_{\mathrm{BS},t} \geq -(E_{\mathrm{BS},t}^{intra} - E_{\mathrm{BS},t}^{ahead}) \tag{64}$$

where $\lambda_{\mathrm{BS}}^{intra}$ is the cost coefficient for the difference between day-ahead and intra-day cost of battery storage.

Similar to battery storage, the intra-day power transactions can be written as:

$$C_{M,t}^{intra} = [\lambda_{M,t} P_{\mathrm{SUB},t} + \lambda_{M,t}^{intra} \Delta E_{M,t}] \Delta t \tag{65}$$

$$s.t. \Delta E_{M,t} \geq E_{M,t}^{intra} - E_{M,t}^{ahead} \tag{66}$$

$$\Delta E_{M,t} \geq -(E_{M,t}^{intra} - E_{M,t}^{ahead}) \tag{67}$$

where $\lambda_{E,t}^{intra}$ is the cost coefficient for the residual of mutual power transaction day-ahead and intra-day cost.

The flow chart for day-ahead and intra-day scheduling problems is shown in Figure 3. The objective function of intra-day scheduling is:

$$min \sum_{t=1}^{T} (C_{\mathrm{CG},t}^{intra} + C_{\mathrm{EH},t}^{intra} + C_{M,t}^{intra} + C_{\mathrm{BS},t}^{intra} + C_{G,t}^{intra} + C_{\mathrm{CO2},t}^{intra} + C_{\mathrm{WT},t}^{intra} + C_{\mathrm{PV},t}^{intra}) \tag{68}$$

where $C_{\mathrm{WT},t}^{intra}$ and $C_{\mathrm{PV},t}^{intra}$ stand for the curtailment penalty of wind and solar energy.

5. Case Study

The proposed method is tested on an MMG, which is structured based on the IEEE 33-bus radial distribution system [32]. Fig. 4 consists of 33 load buses, 2 battery storage systems, 2 controllable generators, 3 wind turbines, 3 photovoltaic generators, and 2 energy hubs, connected to the main grid and the gas network for power and gas transactions. The inner structure of the energy hub is shown in Fig. 5.

The power ratings of CG, WT, and PV are 0.5 MW, 0.8 MW, and 0.8 MW respectively, while the system load-rated active power is 3.715 MW [33]. The electricity (Elect), hydrogen (Hydro), and heat load (Heat) of EH are 0.1 MW, 0.05 MW, and 0.05 MW at node 22 and node 33. The ramp-up and down rates are set in Table 4 and the power ratings of generation and load can be seen in Table 2.

Given the pronounced time delays and substantial thermal losses inherent in long-distance thermal transmission [34], [35], this study adopts a strategy of localized thermal energy supply ignoring the losses. The substation voltage is 12.66 kV and voltage limits $\Delta V_{\max \mathrm{BUS}}$ are set to be $\pm 5\%$ of the nominal level [32], [36].

To exemplify the feasibility of our proposed model. We employ a linearized DistFlow model [37] to attain the optimal voltage profile for the reconstructed IEEE 33-bus MMG by minimizing generation cost while adhering to network constraints Eq. (70) to (73). The resulting optimal voltage profile is visually depicted in Figs. 6, providing a comprehensive illustration of the feasibility and practical application of our devised approach in the realm of electric power systems.

$$\min \sum_{t \in T} C_t \tag{69}$$

$$P_{\mathrm{CG}}^{i,t} + P_{\mathrm{PV}}^{i,t} + P_{\mathrm{WT}}^{i,t} + P_{B,i,t}^{\mathrm{dis,sum}} + P_{\mathrm{SUB}^{i,t}} = P_{\mathrm{P2G}}^{i,t} + P_{\mathrm{TF}}^{i,t} + P_{\mathrm{ET}}^{i,t} + P_{B,i,t}^{\mathrm{ch,sum}} \tag{70}$$

$$V_{i+1,t} = V_{i,t} - (r_{ij}^{\mathrm{line}} P_{ij,t}^{\mathrm{line}} + x_{ij}^{\mathrm{line}} Q_{ij,t}^{\mathrm{line}}) / V_0 \tag{71}$$

$$\underline{V}_i \leq V_{i,t} \leq \overline{V}_i \quad \forall i \in N \tag{72}$$

$$\underline{P}_{ij}^{\mathrm{line}} \leq P_{ij,t}^{\mathrm{line}} \leq \overline{P}_{ij}^{\mathrm{line}} \quad \forall (i,j) \in E \tag{73}$$

Among these, C_t represents the generation cost at time t, while Eq. (70) defines the power balance at node i during time t. The parameters r_{ij}^{line} and x_{ij}^{line} signify the resistance and reactance of branch $i-j$. The variables $\underline{V}_i$ and $\overline{V}_i$ denote the lower and upper limits of the voltage magnitude at node i, respectively. Here, V_0 represents the reference voltage. The terms $P_{ij,t}^{\mathrm{line}}$ and $Q_{ij,t}^{\mathrm{line}}$ correspond to the active power and reactive power of branch $i-j$. The quantities $\underline{P}_{ij}^{\mathrm{line}}$ and $\overline{P}_{ij}^{\mathrm{line}}$ indicate the lower and upper limits of the active power flow on edge $i-j$, respectively. Additionally, T represents the set of hours. N denotes the set of all nodes in the power system, and E represents the set of all edges in the power system.

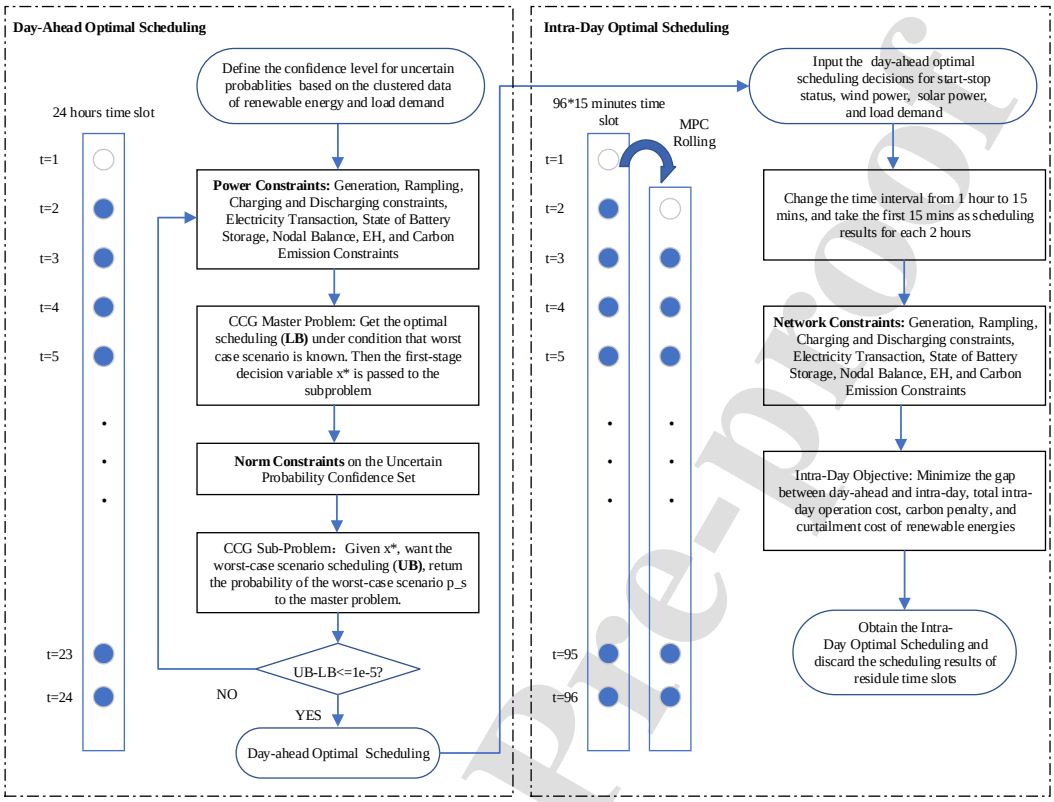

Figure 3: Flow Chart of Day-ahead and Intra-day Scheduling.

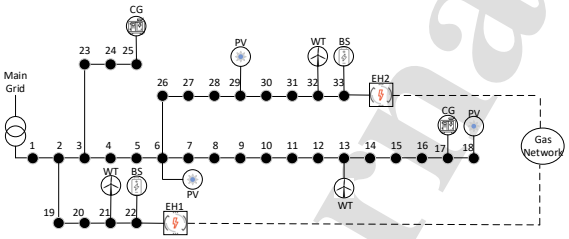

Figure 4: 33-Bus MMG System.

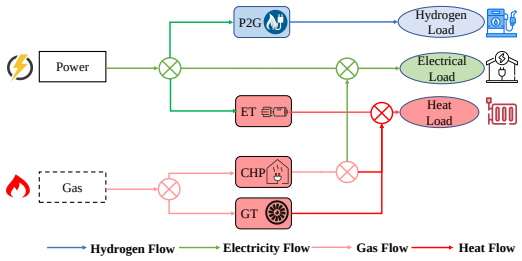

Figure 5: Internal Configuration of an EH.

Table 2
Generation and Load Power Ratings

Unit	WT	PV	CG	Elect	Hydro	Heat
Power (MW)	0.8	0.8	0.5	0.1	0.05	0.05

5.1. DRO Uncertainty Modelling and Settings

At the day-ahead scheduling stage, 24-hour data of 365 scenarios of wind speed and solar intensity are collected, as well as load demand. The K-means method is subsequently employed to cluster 10 representative scenarios. The selection of the clustering center number K is assessed using the silhouette coefficient, thereby reinforcing the robustness of our approach. The silhouette coefficient for a given sample is calculated as (b - a)/max(a, b), where 'a' represents the average distance from the sample to other points within

Table 3
Possibilities of Scenarios

K	1	2	3	4	5	6	7	8	9	10
p_k	0.139	0.073	0.030	0.080	0.022	0.054	0.095	0.098	0.295	0.113

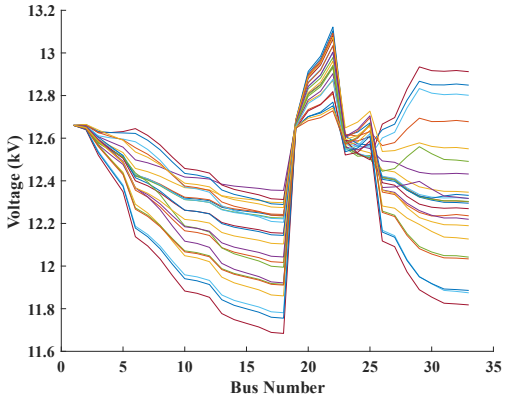

Figure 6: Bus Voltage Variation Over 24 Hours.

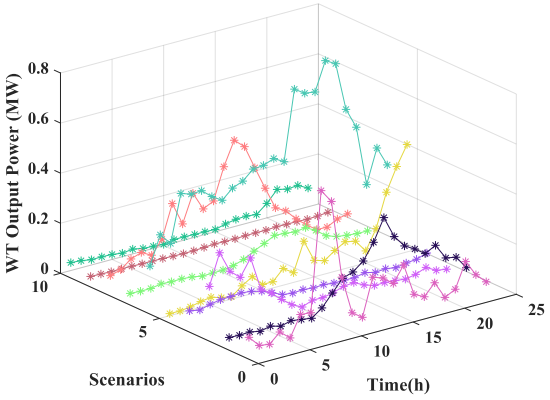

(a) Wind Power Scenarios with Possibility

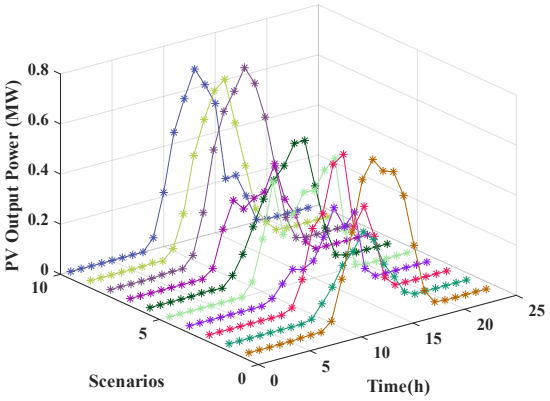

(b) Solar Power Scenarios with Possibility

Figure 7: 10 Clustered Scenarios of RES.

the same cluster, and 'b' denotes the average distance to points in the nearest neighboring cluster [38]. A silhouette coefficient nearing 1 indicates precise sample clustering, whereas proximity to -1 suggests a higher likelihood of samples being inaccurately assigned to the wrong cluster. A silhouette coefficient close to 0 signifies that samples are positioned on the boundary of clusters. For our model with $K = 10$, the computed average silhouette coefficient is 0.82267, which reflects the effectiveness of our approach. Figs. 7 (a) and (b) show the wind and solar power of the 10 clustering scenarios. The initial possibility of each scenario is generated as shown in Table 3. The confidence levels for uncertain probabilities are defined as $\alpha_1 = 0.5$ and $\alpha_\infty = 0.99$.

The power price for bilateral transactions between the main grid and the MMG in the test system, denoted as $\boldsymbol{P}$, are shown in Fig 8. The prices of carbon emissions embedded in the generation of power and gas are defaulted as 0.35 and 0.21 times the power transaction price separately. The gas price is 0.8 times the power price [39]. Moreover, the operation price of a controllable generator is 0.1£/kWh, while the charging and discharging price of battery storage is 0.005£/kWh. The operation cost of the EH is 0.1£/kWh and the start-stop cost is £1000. Details of these parameter settings are shown in Table 4.

The predicted total renewable energy output can be seen in Fig. 9 (a). At 11-14h, the output power of the PV keeps increasing and reaches the peak value of about 1600 kW at around 14h. However, wind power output stays about 200-400 kW all day and reaches peak values at around 8h and 16h. The hydrogen, heat, and electricity loads of the energy hub are shown in Fig. 9 (b). The load of the energy hub keeps

Table 4
Setting of Case Study Parameters

Variable	£/kWh	Variable	kW	Variable	Value
$C^{intra}_{WT,t}$	0.1	$P^{\min/\max}_{B,\mathrm{BS}}$	0/80	$S_{G,t}$	£1000
$C^{intra}_{PV,t}$	0.1	R^{up}/R^{down}	80/80	η_{P2G}	0.6
K_{BS}	0.005	$P^{\min/\max}_{\mathrm{CG}}$	0/300	η_{TF}	0.95
A	0.1	$P^{\min/\max}_{\mathrm{P2G}}$	0/300	η_{ET}	0.7
B	0.1	$P^{\min/\max}_{\mathrm{TF,ET}}$	0/200	η_{GB}	0.7
λ^{intra}_{BS}	0.1	$G^{\min/\max}_{\mathrm{CHP,GB}}$	0/200	η_{ce}	0.4
$\lambda^{intra}_{M,t}$	0.1	$E^{SOC,\min/\max}_{B}$	200/1000	η_{ch}	0.45

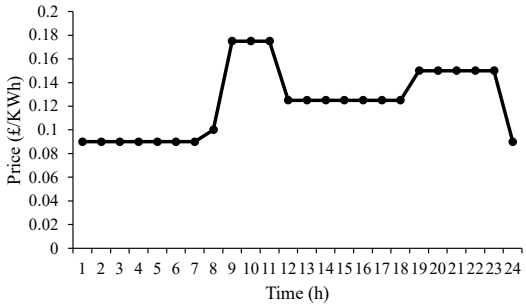

Figure 8: Electricity Price Setting (P).

rising from 6h and reaches its peak value of about 800 kW at around 17h, then decreases steadily to 250-300 kW. The total nodal load in the test system is depicted in Fig. 9 (c). It is obvious that there are two peaks at around 11h and 21h, which are both about 2250kW.

5.2. Day-Ahead Results and Discussion

In the day-ahead operation, initial worst-case expectations are predicated on ten representative scenarios with corresponding probabilities, thereby setting the groundwork for the first iterative application of C&CG to day-ahead optimization. The optimal scheduling, depicted in Fig. 10, demonstrates strategic energy management across different hours of the day. During peak load periods, around 9h and 21h, controllable generators exhibit maximum output, nearly 900kW, ensuring sufficient power supply. Concurrently, the microgrid draws electricity from the primary grid during off-peak hours, namely between 1-10h and 15-24h, correlating with a relatively high level of carbon emissions.

As Fig. 10 shows, around 9h and 21h, the total output of controllable generators reaches the peak value of about 900kW, providing enough power during the period when the load reaches its peak value. Also, during 1-10h and 15-24h, the microgrid draws electricity from the main grid. At the same time, the amount of carbon emitted is relatively high during the day accordingly. Conversely, the microgrid sells electricity to the main grid over 11-15h corresponding to the period that the RES generates the maximum power. Consequently, the overall carbon emissions reach the valley value because of the high output of the RES.

Conversely, the microgrid exports power back to the main grid from 11-15h, which is the period of peak RES production. This results in a significant dip in carbon emissions due to the substantial RES output. Meanwhile, the battery storage system displays two significant charging peaks at around 8h and 20h, which are associated with the times when the CG is operating at its highest capacity and the microgrid purchases a considerable amount of electricity from the main grid. However, the battery discharges during 8-11h and 15-24h, in line with the periods of decreased RES output. This behavior demonstrates the critical role of the battery system in supplementing the CG during high load demands, ensuring a well-balanced and efficient microgrid operation.

5.3. Result Comparison with RO/SO Methods

To showcase the advantages of the DRO approach, it is essential to draw comparisons with both RO and SO methods. In this context, we consider the worst-case scenario outcome as the optimal scheduling result for RO, while for SO, we obtain the optimal scheduling by approximating a normal distribution for the probability distribution in the clustered 10 typical scenarios. This comparative analysis serves as a means to highlight the advantages of the DRO approach in effectively addressing uncertainties inherent in optimization problems.

In Fig. 11 (a) and (b), we present the optimal scheduling results for RO and SO. The trends among the three methods are observed to be similar, yet notable differences persist. Specifically, the overall CG output under RO is the lowest, amounting to 11820 KWh, while its power purchase is the highest at 14864.71 KWh. In contrast, the overall CG output under SO is the highest at 12185.49 KWh, and the corresponding power purchase is the lowest at 14499.25 KWh.

This indicates that the MMG produces less electricity and relies more on power purchases from the main grid under RO, whereas it produces more and purchases less under SO. As DRO results lie between RO and SO, it implies that DRO achieves greater savings than RO while adopting a more conservative approach than SO. To enhance the clarity of the advantages of DRO, we have conducted a quantified cost and carbon emissions comparison of RO and SO in Table 5. The results show that RO yields the highest cost, while SO incurs the lowest expenses. Meanwhile, DRO falls between RO and SO in terms of cost implications, further signifying that DRO strikes a balance between the conservative attributes of RO and the economic efficiency associated with SO.

Table 5
Result Comparison of Solving Methods

Methods	Cost with CP (£)	Carbon Emissions (kg)
RO	6405.97	21981.73
DRO	6279.81	22053.65
SO	6023.19	22221.65

5.4. Effects of Employing EH

To illustrate the advantages of employing EH, generation is bifurcated to cater to distinct loads, as highlighted in [40]. In this case, the CHP unit is partitioned into two segments. Electricity and heat loads are independently provided by gas-fired power plants and boilers with higher energy conversion efficiencies, which are 0.53 and 0.8 as mentioned in [40]. The internal configuration of the EH system is modified, as depicted in Fig. 12. It is assumed that the operational costs of the CHP unit are equivalent to those of the power plant and boiler, with the gas price set at 0.8 times the power transaction price.

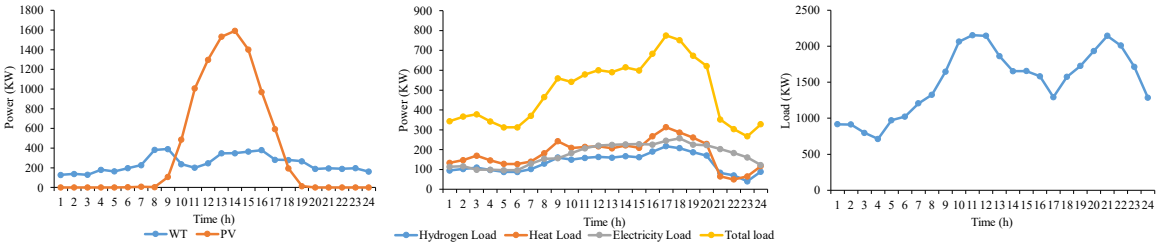

(a) RES Power Day-ahead Prediction (b) EH Load Day-ahead Prediction (c) Total Nodal Load Day-ahead Prediction

Figure 9: Day-Ahead Prediction Results.

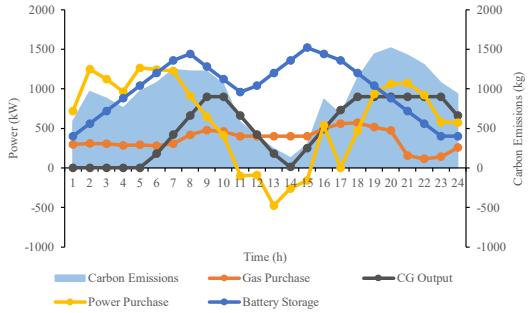

Figure 10: Day-Ahead DRO Scheduling Results.

The presented findings, as delineated in Table 6, distinctly manifest a consequential increase in both total cost and carbon emissions when the CHP system is omitted from the energy framework. Specifically, the absence of CHP leads to a significant rise of £62 in total costs and an increase of 950 kg in carbon emissions, notwithstanding the fact that the power plant and boiler exhibit higher energy conversion efficiencies compared to the CHP. This observed phenomenon underscores the capacity of CHP to capitalize on residual energy, converting it into a usable form, thereby substantially enhancing overall energy utilization within the power system [41]. In a broader context, the incorporation of CHP emerges as a potent driver for expediting the critical endeavor of decarbonization.

Table 6
Cost and Carbon Impacts of CHP

Impacts of CHP	No CHP	With CHP
Cost (£)	6341.58	6279.80
Carbon Emissions (kg)	23002.60	22053.65

5.5. Impacts of Carbon Penalty

From Fig. 13 (a), the carbon emissions decrease significantly when considering the CP between 10-18h (hours 10 to 18), a period characterized by relatively high load demand for EH in Fig. 9 (b). That is because the operator prefers to use cleaner energy sources like wind and solar power, which can be stored in a battery, rather than using energy sources that produce more carbon emissions to meet the electricity and heat demands. Therefore, the battery in Fig. 13 (c) would store the excess power instead of selling it to the main grid, which can be seen in Fig. 13 (d). Accordingly, the gas purchase in Fig. 13 (b) goes down slightly because the EH prefers cleaner energies to supply the electricity and heat loads. Meanwhile, the output of controllable generators in Fig. 13 (e) decreases greatly even though the demand is high during that time.

To represent the effects of CP , Table 7 is shown, where with CP, the total carbon emissions of one day are reduced by 2.6t while the day cost increases by £1560. Overall, it underscores the significant potential of CP in facilitating substantial reductions in carbon emissions.

Table 7
Cost and Carbon Impacts of CP.

Day-Ahead Results	Cost (£)	Carbon Emissions (kg)
No CP	4719.24	24676.633
With CP	6279.80	22053.653

In addition, it is discernible that alterations in carbon pricing have contrasting effects on both the total cost and carbon emissions. To investigate the effects of carbon pricing, we have introduced variations in carbon prices based on multiples of P, leading to distinct outcomes. Table 8 shows the embedded carbon prices for both power and gas generation, alongside the ensuing optimal scheduling costs. This analysis contributes to a more comprehensive understanding of the dynamics associated with carbon pricing within the context of our study, by employing the random sampling methodology [42].

The results among five cases clearly show that the total cost rises with increasing carbon price in Table 8. In order to comprehensively assess the effects of varying carbon prices on additional cost factors, a broader spectrum of data comparisons is required. Fig. 14 provides an illustrative representation of the trends in total carbon emissions, power transactions, CG output, gas purchases, and battery storage across multiple scenarios over a full day. This analysis

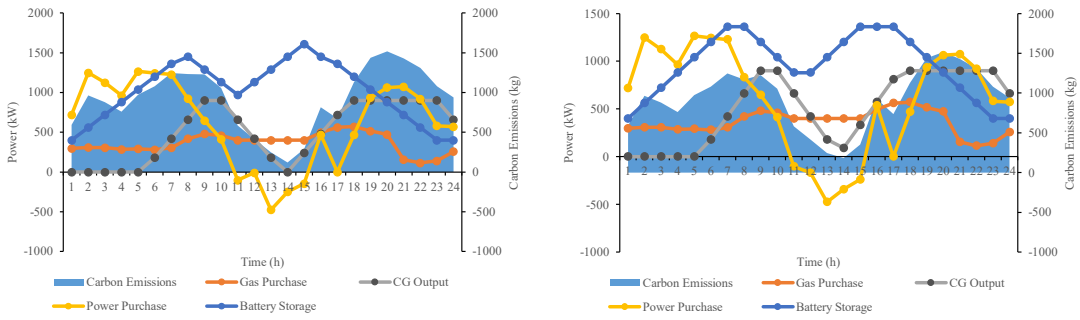

(a) Robust Optimal Scheduling Results

(b) Stochastic Optimal Scheduling Results

Figure 11: Robust and Stochastic Scheduling Results.

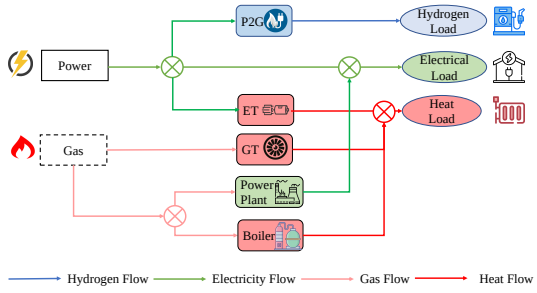

Figure 12: Internal Configuration of EH without CHP.

Table 8
Carbon Penalty of Power and Gas under Different Cases

$\times P$	Case1	Case2	Case3	Case4	Case5
P_{cp}	0.21	0.28	0.35	0.42	0.49
P_{cg}	0.07	0.14	0.21	0.28	0.35
Cost (£)	5615.96	5952.15	6279.80	6603.41	6911.46

contributes to a more comprehensive understanding of the dynamics associated with carbon pricing within the context of this study.

In Fig. 14, the observed slight increase in power transactions is not indicative of the microgrid procuring more electricity from the main grid; rather, it results from a reduction in power sold by the microgrid to the main grid, enabling more energy storage for self-consumption. Consequently, the overall volume of power transactions slightly increases. Conversely, there is a general decline in carbon emissions, gas purchases, and CG output. Additionally, the SOC of the battery diminishes, as it needs to discharge energy to meet the prevailing load demands.

Interestingly, the carbon emission stays the same in Cases 1 and 2 as well as Cases 4 and 5 even though the total costs of Cases 2 and 5 are higher than those of Cases 1 and 4. And the same phenomenon happens with power transactions, gas purchases, and CG output. The reason is that the total load demand is unchanged among these cases. Moreover, the CP cost may account for less weight than other costs. It can be concluded that Case 4 is the overall optimal carbon price setting that achieves the lowest carbon emission with less cost than Case 5.

In [26], the carbon price stays the same over the whole day. To analyze the impact of time-varying versus constant carbon pricing, a comparison is made using the results from Case 4, as previously discussed, where the CP price for power and gas stands at 0.42 and 0.28 times of the transaction price, respectively. The average daily prices for power and gas, which amount to £0.0520 and £0.0347, respectively, are considered. Table 9 reveals that the application of time-varying carbon pricing yields lower carbon emissions at the expense of higher costs compared to a constant carbon price in this case study. This analysis offers valuable insights that can aid utility companies in devising strategies tailored to specific requirements and objectives.

Table 9
Comparison between Time-Varying and Constant Carbon Prices.

Carbon Price	Cost (£)	Carbon Emissions (kg)
Time-Varying	6603.41	21751.75
Constant	6551.68	21766.15

5.6. Intra-Day Results and Discussions

To illustrate the feasibility of real-time intra-day scheduling, the intra-day predictions and results are discussed in this section. The comparison of day-ahead and intra-day predictions for solar and wind energy as well as the total load can be seen in Fig. 15. (a) and (b) represent the forecasts for PV and WT output, respectively, while (c) indicate the load predictions. It is evident that there are observable minor differences between intra-day and day-ahead predictions.

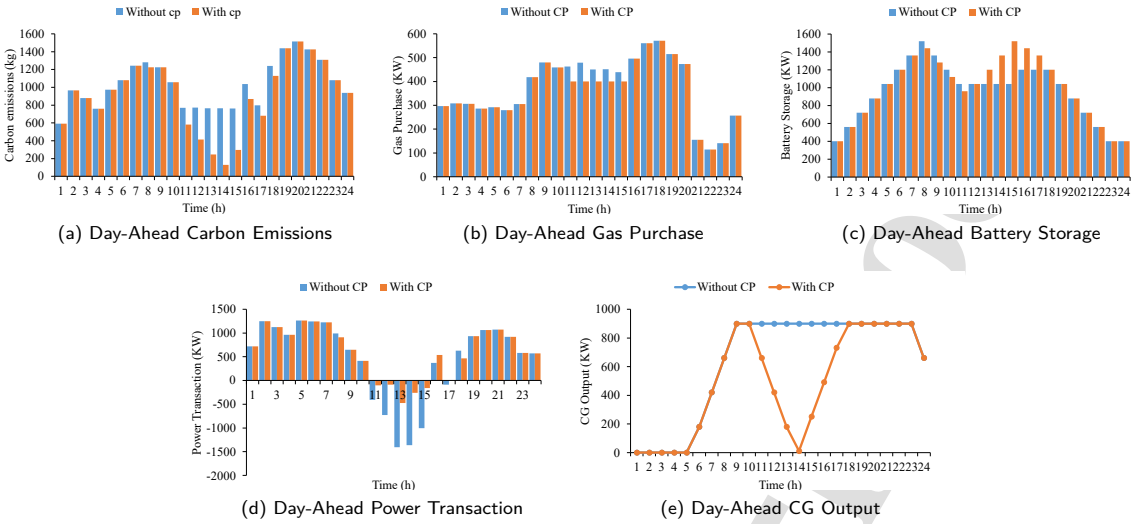

(a) Day-Ahead Carbon Emissions (b) Day-Ahead Gas Purchase (c) Day-Ahead Battery Storage

(d) Day-Ahead Power Transaction (e) Day-Ahead CG Output

Figure 13: Day-Ahead Scheduling Results Comparison Under Conditions With And Without Carbon Penalty.

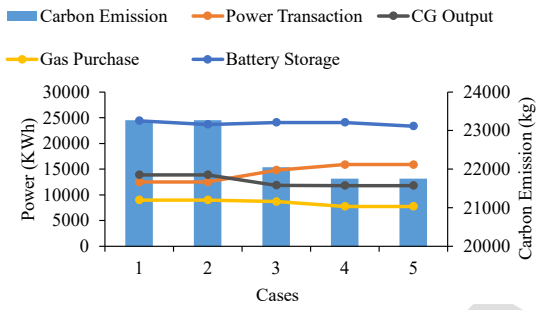

Figure 14: Carbon Penalty Impacts over 5 Cases.

The intra-day outputs of renewable energies are slightly higher than day-ahead predictions at around 9h and 18h, while intra-day load predictions generally show a slightly lower magnitude compared to day-ahead predictions around 8h and 21h. This reflects the robustness of the day-ahead scheduling.

The optimal intra-day scheduling is shown in Fig. **??**. The intra-day results should ideally closely follow the day-ahead decision. As seen in the figure, the overall trends of intra-day and day-ahead scheduling are generally consistent. However, there are some moments where slight differences exist due to variations in day-ahead and intra-day renewable energy and load forecasts. During the low RES and high load demand period around 9h and 21h mentioned in Section 5.2, the utility procures more gas to accommodate the elevated heat load. Given that the CP price is lower than the power transaction price, the utility's inclination is to sell surplus power to the main grid for higher overall revenue, despite the associated increase in carbon emissions. In general, the intra-day scheduling effectively aligns with the preceding scheduling decisions. With a shorter time scale and swift response, it can adeptly accommodate dynamic changes in natural and human-induced uncertainties.

When considering the CP for intra-day scheduling, the total cost of intra-day scheduling is £6964.36, while the intra-day cost without CP is £5359.72. Additionally, the carbon emissions have been reduced by over 1100 kg. Both cost and carbon emissions data for intra-day scheduling are presented in Table 10. This observation underscores the pronounced impact of decarbonizing strategies once again. From the results of both day-ahead and intraday scheduling, this multi-timescale scheduling method provides a decarbonizing and robust optimized scheduling solution for MMGs.

Table 10
Intra-day Carbon Penalty Impact.

Intra-day Results	Cost (£)	Carbon Emissions (kg)
No Carbon Penalty	5359.72	22033.13
With Carbon Penalty	6964.36	20136.56

6. Conclusion

This paper introduces a novel operational framework for MMG that emphasizes low-carbon sustainability and addresses uncertainties in solar and wind energy generation, along with demand fluctuations. The framework's primary objective is to optimize decarbonization by concurrently minimizing operational costs and mitigating carbon penalty expenses. To address this optimization challenge, we propose a unique multi-temporal approach grounded in data-driven DRO. Our key aim is to create an hourly

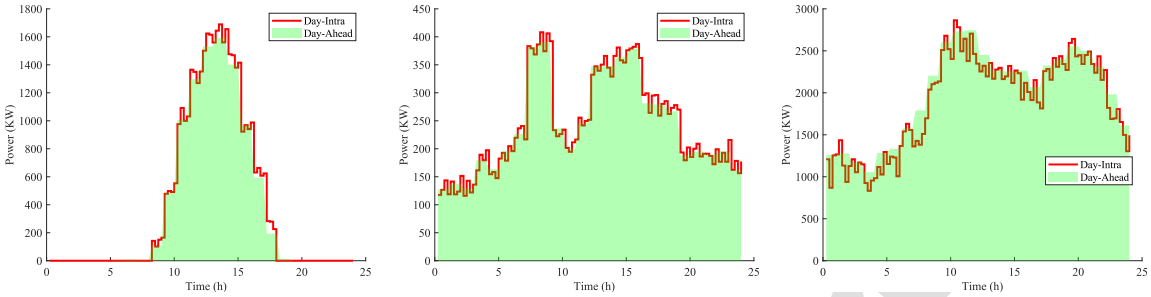

(a) PV Output Prediction (b) WT Output Prediction (c) Total Load Prediction

Figure 15: Comparison between Day-ahead and Intra-day Power and Load Prediction.

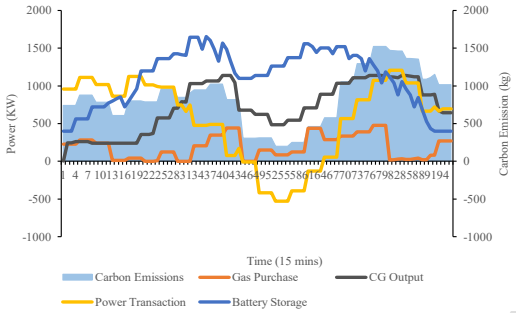

Figure 16: Intra-day Optimal Scheduling Results.

day-ahead optimal scheduling framework that seamlessly integrates considerations of economic efficiency and robustness within the context of decarbonization. Furthermore, we demonstrate the practicality of real-time dispatch in 15-minute intervals by presenting intra-day operations within our case study. To effectively confront the challenges posed by significant uncertainties, we adopt a comprehensive approach. This includes the utilization of clustering techniques to derive representative scenarios from empirical data on renewable energies and load demand, all while accounting for the ambiguity set within the probability distribution.

Validation of this model and framework was conducted through testing on the IEEE 33-bus distribution network, from which several key findings have emerged: 1) Within the framework of the multi-energy microgrid featuring CHP technology, a commendable reduction of 9.5t in carbon emissions is observed, coupled with a lower cost saving amounting to £61.78. 2) Notably, under the CP condition, a significant reduction in carbon emissions, amounting to 10.6%, has been attained. 3) The alignment between intra-day 15-minute scheduling and day-ahead hourly scheduling is demonstrated, addressing the stochastic nature of renewable energy sources at various stages through multi-temporal scheduling approaches which enhances the integration of renewable energy and leads to carbon reduction.

In conclusion, our study uses advanced methods to address uncertainties in the MMG, with a focus on reducing carbon emissions and energy consumption. Key contributions include the effective use of data-driven DRO for improved energy utilization in the microgrid. The optimization framework highlights the efficacy of carbon penalty pricing mechanisms, and the proposed approach considers multi-temporal uncertainties, reducing operational costs and enhancing MMG reliability. Overall, our study provides a practical framework for achieving low-carbon and energy-saving outcomes in microgrid management. In future research endeavors, it is essential to explore improvements that address the dynamic challenges inherent in integrating renewable energy and managing power grids. This involves a thorough consideration of intricate details within the power grid infrastructure to enhance overall system efficiency and reliability.

References

[1] R. K. Sinha, N. D. Chaturvedi, A review on carbon emission reduction in industries and planning emission limits, Renewable and Sustainable Energy Reviews 114 (2019) 109304.

[2] M. S. Ziegler, J. M. Mueller, G. D. Pereira, J. Song, M. Ferrara, Y.-M. Chiang, J. E. Trancik, Storage requirements and costs of shaping renewable energy toward grid decarbonization, Joule 3 (9) (2019) 2134–2153.

[3] H. Quan, D. Srinivasan, A. M. Khambadkone, A. Khosravi, A computational framework for uncertainty integration in stochastic unit commitment with intermittent renewable energy sources, Applied energy 152 (2015) 71–82.

[4] P. Mancarella, Mes (multi-energy systems): An overview of concepts and evaluation models, Energy 65 (2014) 1–17.

[5] M. Mohammadi, Y. Noorollahi, B. Mohammadi-Ivatloo, H. Yousefi, Energy hub: From a model to a concept–a review, Renewable and Sustainable Energy Reviews 80 (2017) 1512–1527.

[6] D. Bertsimas, V. Gupta, N. Kallus, Data-driven robust optimization, Mathematical Programming 167 (2018) 235–292.

[7] Y. Xiang, J. Liu, Y. Liu, Robust energy management of microgrid with uncertain renewable generation and load, IEEE Transactions on Smart Grid 7 (2) (2016) 1034–1043. doi:10.1109/TSG.2014.2385801.

[8] F. Shen, L. Zhao, W. Du, W. Zhong, F. Qian, Large-scale industrial energy systems optimization under uncertainty: A data-driven robust optimization approach, Applied Energy 259 (2020) 114199.

[9] Q. Jiang, M. Xue, G. Geng, Energy management of microgrid in grid-connected and stand-alone modes, IEEE transactions on power

systems 28 (3) (2013) 3380–3389.
[10] H. Kanchev, F. Colas, V. Lazarov, B. Francois, Emission reduction and economical optimization of an urban microgrid operation including dispatched pv-based active generators, IEEE Transactions on sustainable energy 5 (4) (2014) 1397–1405.
[11] L. Meng, E. R. Sanseverino, A. Luna, T. Dragicevic, J. C. Vasquez, J. M. Guerrero, Microgrid supervisory controllers and energy management systems: A literature review, Renewable and Sustainable Energy Reviews 60 (2016) 1263–1273.
[12] Z. Li, Y. Xu, Optimal coordinated energy dispatch of a multi-energy microgrid in grid-connected and islanded modes, Applied Energy 210 (2018) 974–986.
[13] Z. Chen, Y. Zhang, W. Tang, X. Lin, Q. Li, Generic modelling and optimal day-ahead dispatch of micro-energy system considering the price-based integrated demand response, Energy 176 (2019) 171–183.
[14] Z. Tan, S. Yang, H. Lin, G. De, L. Ju, et al., Multi-scenario operation optimization model for park integrated energy system based on multi-energy demand response, Sustainable Cities and Society 53 (2020) 101973.
[15] Z. Li, Y. Xu, Dynamic dispatch of grid-connected multi-energy microgrids considering opportunity profit, in: 2017 IEEE Power & Energy Society General Meeting, IEEE, 2017, pp. 1–5.
[16] L. He, Z. Lu, L. Geng, J. Zhang, X. Li, X. Guo, Environmental economic dispatch of integrated regional energy system considering integrated demand response, International Journal of Electrical Power & Energy Systems 116 (2020) 105525.
[17] Z. Li, B. Zhao, Z. Chen, C. Ni, J. Yan, X. Yan, X. Bian, N. Liu, Low-carbon operation method of microgrid considering carbon emission quota trading, Energy Reports 9 (2023) 379–387.
[18] X. Zhong, W. Zhong, Y. Liu, C. Yang, S. Xie, Optimal energy management for multi-energy multi-microgrid networks considering carbon emission limitations, Energy 246 (2022) 123428.
[19] A. Coelho, J. Iria, F. Soares, J. P. Lopes, Real-time management of distributed multi-energy resources in multi-energy networks, Sustainable Energy, Grids and Networks 34 (2023) 101022.
[20] X. Guan, Z. Xu, Q.-S. Jia, Energy-efficient buildings facilitated by microgrid, IEEE Transactions on smart grid 1 (3) (2010) 243–252.
[21] S. E. Ahmadi, D. Sadeghi, M. Marzband, A. Abusorrah, K. Sedraoui, Decentralized bi-level stochastic optimization approach for multi-agent multi-energy networked micro-grids with multi-energy storage technologies, Energy 245 (2022) 123223.
[22] Z. Li, Y. Xu, Temporally-coordinated optimal operation of a multi-energy microgrid under diverse uncertainties, Applied energy 240 (2019) 719–729.
[23] A. A. Lekvan, R. Habibifar, M. Moradi, M. Khoshjahan, S. Nojavan, K. Jermsittiparsert, Robust optimization of renewable-based multi-energy micro-grid integrated with flexible energy conversion and storage devices, Sustainable Cities and Society 64 (2021) 102532.
[24] Z. Shi, T. Zhang, Y. Liu, Y. Feng, R. Wang, S. Huang, Optimal design and operation of islanded multi-microgrid system with distributionally robust optimization, Electric Power Systems Research 221 (2023) 109437.
[25] J. Jin, P. Zhou, C. Li, X. Guo, M. Zhang, Low-carbon power dispatch with wind power based on carbon trading mechanism, Energy 170 (2019) 250–260.
[26] X. Zhang, Z. Liang, S. Chen, Optimal low-carbon operation of regional integrated energy systems: A data-driven hybrid stochastic-distributionally robust optimization approach, Sustainable Energy, Grids and Networks 34 (2023) 101013.
[27] Y. Shui, J. Liu, H. Gao, S. Huang, Z. Jiang, A distributionally robust coordinated dispatch model for integrated electricity and heating systems considering uncertainty of wind power, Proceedings of the CSEE 38 (24) (2018) 7235–7247.
[28] T. Ding, Q. Yang, Y. Yang, C. Li, Z. Bie, F. Blaabjerg, A data-driven stochastic reactive power optimization considering uncertainties in active distribution networks and decomposition method, IEEE Transactions on Smart Grid 9 (5) (2017) 4994–5004.
[29] B. Zeng, L. Zhao, Solving two-stage robust optimization problems using a column-and-constraint generation method, Operations Research Letters 41 (5) (2013) 457–461.
[30] Y. He, Z. Li, J. Zhang, G. Shi, W. Cao, Day-ahead and intraday multi-time scale microgrid scheduling based on light robustness and mpc, International Journal of Electrical Power & Energy Systems 144 (2023) 108546.
[31] J. Wang, J. Sui, H. Jin, An improved operation strategy of combined cooling heating and power system following electrical load, Energy 85 (2015) 654–666.
[32] C. Zhang, Y. Xu, Z. Y. Dong, K. P. Wong, Robust coordination of distributed generation and price-based demand response in microgrids, IEEE Transactions on Smart Grid 9 (5) (2017) 4236–4247.
[33] M. A. Kashem, V. Ganapathy, G. Jasmon, M. Buhari, A novel method for loss minimization in distribution networks, in: DRPT2000. International conference on electric utility deregulation and restructuring and power technologies. Proceedings (Cat. No. 00EX382), IEEE, 2000, pp. 251–256.
[34] W. Gu, J. Wang, S. Lu, Z. Luo, C. Wu, Optimal operation for integrated energy system considering thermal inertia of district heating network and buildings, Applied energy 199 (2017) 234–246.
[35] L. Ma, N. Liu, J. Zhang, W. Tushar, C. Yuen, Energy management for joint operation of chp and pv prosumers inside a grid-connected microgrid: A game theoretic approach, IEEE Transactions on Industrial Informatics 12 (5) (2016) 1930–1942.
[36] C. Zhang, Y. Li, Thermodynamic performance of cycle combined large temperature drop heat exchange process: Theoretical models and advanced process, Energy 150 (2018) 1–18.
[37] S. Lu, Y. Li, W. Gu, Y. Xu, S. Ding, Economy-carbon coordination in integrated energy systems: Optimal dispatch and sensitivity analysis, Applied Energy 351 (2023) 121871.
[38] K. R. Shahapure, C. Nicholas, Cluster quality analysis using silhouette score, in: 2020 IEEE 7th International Conference on Data Science and Advanced Analytics (DSAA), 2020, pp. 747–748. doi:10.1109/DSAA49011.2020.00096.
[39] Scottish power tariff information.
URL https://www2.scottishpower.co.uk/tariff-information.process?execution=e1s8
[40] A. Martens, The energetic feasibility of chp compared to the separate production of heat and power, Applied thermal engineering 18 (11) (1998) 935–946.
[41] L. Zhang, F. Li, B. Sun, C. Zhang, Integrated optimization design of combined cooling, heating, and power system coupled with solar and biomass energy, Energies 12 (4) (2019) 687.
[42] S. K. Thompson, Sampling, Vol. 755, John Wiley & Sons, 2012.

Miaorui Ma: Conceptualization, Validation, Methodology, Software, Investigation, Writing - Original Draft

Chengwei Lou: Supervision, Conceptualization, Investigation, Writing - Review & Editing

Xiangmin Xu: Conceptualization, Writing - Review & Editing

Jin Yang: Supervision, Project administration, Writing - Review & Editing

Jake Cunningham: Writing - Review & Editing

Lu Zhang: Writing - Review & Editing

Declaration of interests

☒ The authors declare that they have no known competing financial interests or personal relationships that could have appeared to influence the work reported in this paper.

☐ The authors declare the following financial interests/personal relationships which may be considered as potential competing interests: